ELSEVIER

Journal of Structural Geology 28 (2006) 323–332

JOURNAL OF STRUCTURAL GEOLOGY

www.elsevier.com/locate/jsg

Fault gouge evolution in highly overconsolidated claystones

Marc Holland [a,*], Janos L. Urai [a], Wouter van der Zee [a,b], Helge Stanjek [c], Jan Konstanty [d]

[a] *Geologie/Endogene Dynamik–RWTH Aachen, Lochnerstrasse 4-20, D-52056 Aachen, Germany*
[b] *GeoMechanics International, Emmerich Josef Strasse 5, D-55116 Mainz, Germany*
[c] *Mineralogie/Tonmineralogie und Petrologie–RWTH Aachen, Wüllnerstraße 2, D-52062 Aachen, Germany*
[d] *Petroleum Development Oman, P.O. Box 81, Postal Code 11, Muscat, Sultanate of Oman*

Received 5 January 2005; received in revised form 30 September 2005; accepted 4 October 2005
Available online 7 November 2005

Abstract

Processes of fault gouge evolution in hard claystones start with cataclasis that produces a soft clay gouge which fills the space between the initial fragments. This re-seals the initially highly porous and permeable damage zone, without diagenetic processes. We studied this process in shales and sandstones, deformed in normal faults after uplift to shallow crustal depths in the Ardennes and Eifel. Detailed mapping shows four different lithotypes from intact shale in the wall rock, broken wall rock fragments with various amounts of clay, to a fully reworked gouge. These lithotypes reflect different evolutionary stages. The similar mineralogy of the different lithotypes suggests that the main process involved is mechanical fragmentation with minor contribution by diagenetic changes or weathering, accompanied by large changes in microstructure, porosity and transport properties. While the wall rock has a very low porosity and permeability, initial deformation results in a much higher porosity with large pores. The reworked clay gouge also has a high porosity, but its pore size corresponds to a lower permeability and higher capillary seal capacity. In upper crustal fault zones in strong, brittle lithologies, this early re-sealing in sections consisting of claystone will lead to local barriers to along-fault fluid flow.

Keywords: Gouge; Overconsolidated claystone; Faulting

1. Introduction

Faulting usually leads to large changes in mechanical and transport properties of a rock body. In the early stages of deformation, processes of fault gouge evolution depend on mineralogy, porosity and cohesive strength of the wall rock, effective stress path, temperature and chemical composition and flow velocity of the pore fluid (Knipe, 1992; Chester, 1993; Caine et al., 1996; Evans et al., 1997). For example, porous sandstone, claystone or limestone deforming under sufficiently high effective stress may compact during deformation, while the same rock may dilate when deformed under lower effective stress (Lambe and Whitman, 1969; Rawling, 2001a; Vajdova et al., 2004). This process will lead to large changes in shear strength and transport properties (Evans et al., 1997), and a complex evolution of the fault zone with increasing displacement (Chester, 1993; Caine et al., 1996; Shipton and Cowie, 2001). The contrast between properties of fault gouge and wall rock is largest when the wall rock has previously been compacted and cemented at depth much higher than that of the faulting. This overconsolidation will lead to initial dilatant faulting, and to a fault gouge, which has a higher porosity and much lower relative strength than the wall rock. In these faults, the initial increase in permeability (Evans et al., 1997; Wibberley and Shimamoto, 2003) commonly leads to diagenetic reactions, which may produce new minerals (Kralik et al., 1987) or lead to precipitation in veins or pores with associated reduction of permeability and partial restoration of shear strength. While in sandstones (Rawling, 2001b; Shipton and Cowie, 2001) and carbonates (Mollema and Antonellini, 1999; Billi et al., 2002), many aspects of this process have been documented, processes in hard claystones (Nüesch and Baumann, 1989; Nüesch, 1991; Urai and Wong, 1994; Olgaard et al., 1995) are poorly known. An interesting aspect here is that progressive deformation of a hard shale can be expected to result in grain-scale disintegration of the rock and produce a soft clay

* Corresponding author.
E-mail address: m.holland@ged.rwth-aachen.de (M. Holland).

0191-8141/$ - see front matter © 2005 Elsevier Ltd. All rights reserved.
doi:10.1016/j.jsg.2005.10.005

in critical state (Jones and Addis, 1986; Jones, 1994). This gouge has a higher porosity and significantly lower strength than the wall rock, and forms without the need for diagenetic processes. Although it is more permeable than the country rock, if it fills the voids of the fault zone, it can form a seal for fluid flow (Hildenbrand and Urai, 2003). An example of this process is described by Lindsay (1993) for normal faults in a highly overconsolidated sand–clay sequence. Here, the fault gouge is dominantly composed of soft, reworked clay gouge, which can form a clay smear between juxtaposed sandstone layers. However, although the basic processes were recognized, a detailed microstructural and petrophysical study of the process was not reported in this study. The aim of this paper is to document the evolution of microstructure and the corresponding transport properties in a fault zone forming in hard claystones, based on outcrop study, and laboratory analysis of samples taken in the field.

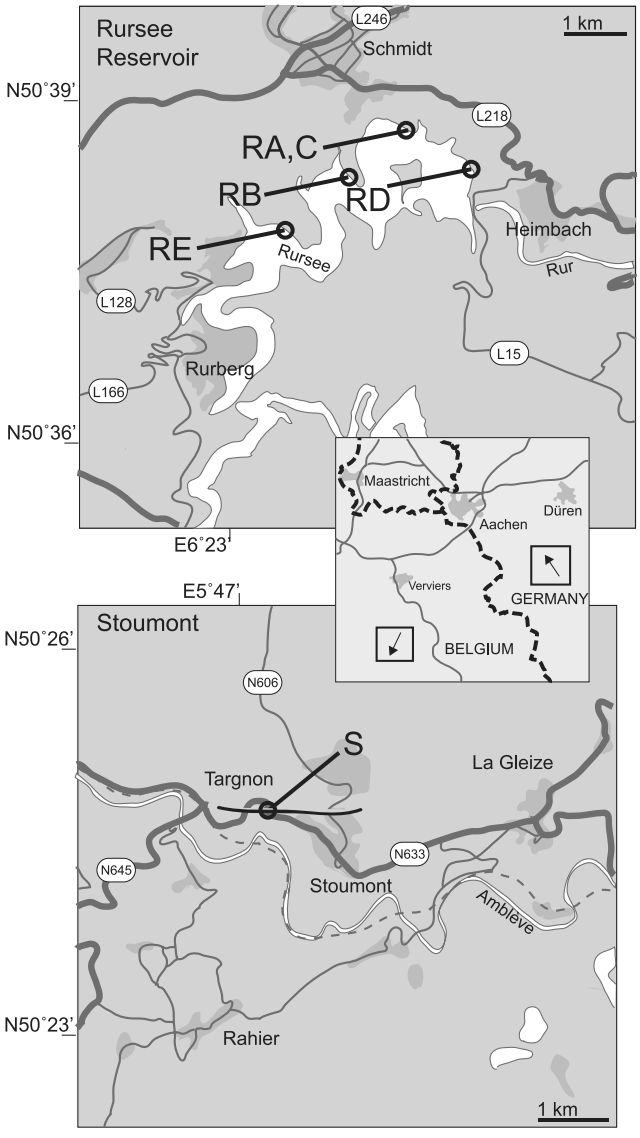

Fig. 1. Geographic location of the two outcrop sites at the Rursee reservoir in the German Eifel (R) and Stoumont in the Belgian Ardennes (S).

2. Geological setting

The outcrops studied are located in the Variscan foreland thrust belt in the Ardennes and Eifel (Walter, 1992). The rocks are sandstones and fissile claystones. Burial of the rocks in a passive continental margin to depths of around 8 km (T and P around 300 °C and 200 MPa (Kramm, 1982)) and the subsequent Variscan orogeny produced a typical sequence of hard claystones and sandstones and led to the development of reverse faults and folds with associated cleavage. This was followed by uplift, erosion and post-orogenic faulting (Walter, 1992). After the formation of a peneplain and cretaceous sedimentation, uplift of the Rhenish massif started in the Upper Cretaceous and has continued to recent times. A post-Oligocene uplift of up to 460 m can be demonstrated in parts of the area (Walter, 1992). The differential uplift between distinct blocks (Fuchs et al., 1983) led to the formation of normal faults and to reactivation of existing structures. The normal fault systems described in this paper were probably formed in this last stage.

3. Outcrop characteristics

The first outcrop (Fig. 1; Stoumont/Belgium, at the N633 road between Targnon and Stoumont) is located in the Cambro-Ordovician basement, in the other (Fig. 1; Rursee reservoir/Germany (Wunstorf, 1928)) the rocks are of lower Devonian age (Walter and Wohlenberg, 1985). The outcrops studied comprise interbedded sandstone and shale layers and normal faults with clay gouge. The fault structures in all outcrops are very similar and are described together; reference to individual locations is given in the figure captions. The faults are usually sub parallel to the local orientation of bedding and are located close to the shale/sandstone interface. This setting is usually found on the folds limbs. Cross-cutting relationships are, in contrast, present in the proximity of fold-hinges. The fault zones show large variations in their width, between a few centimetres and 1 m (Fig. 2). A prominent thin clay gouge with a rather sharp contact to the wall rock can change gradually in a wide fault zone composed of damaged wall rock and multiple strands of gouge. A clearly defined fault core between damage zones (Chester, 1993; Caine et al., 1996; Gudmundsson et al., 2001) is not present as expected for a fully localized mature fault. Soft gouge is found in a complex network of anastomosing or branching strands, heterogeneously distributed in a wider zone of disrupted wall rock.

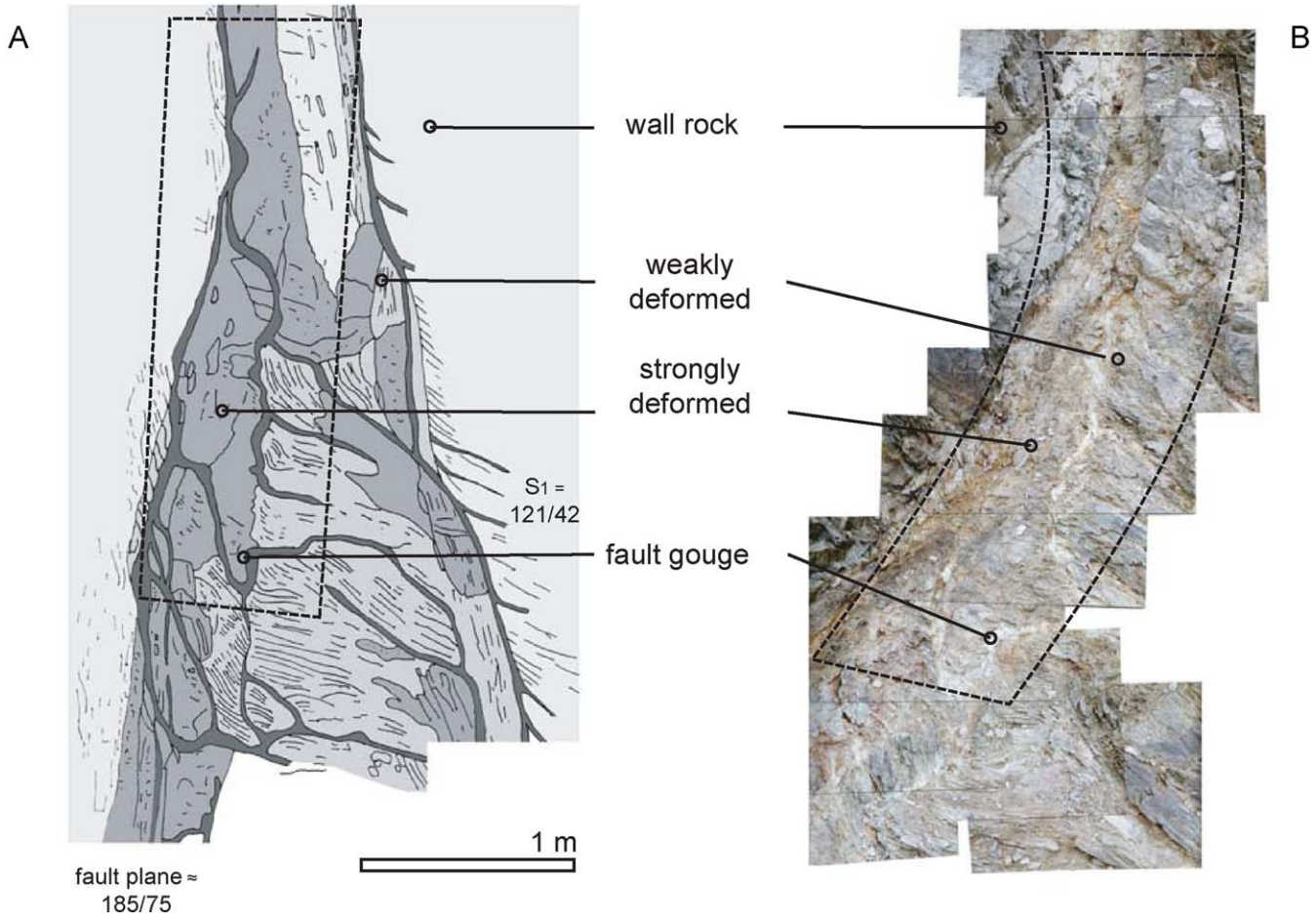

Fig. 2. Details of the Rursee B outcrop (RB) shown as a photo collage (B) and as field-interpretation (A). The fault zone is sub-parallel to the bedding of a claystone/sandstone sequence. The fault zone width is variable and shows a heterogeneous assemblage of strands of fault gouge and differently deformed claystone material. Localization towards a single slip-plane is not evident. At favourable locations, gouge strands branch into the shistosity (boxes for orientation).

4. Methods

The outcrops (example shown in Fig. 2) were carefully cleaned with tungsten carbide scrapers, photographed, mapped in detail and sampled using steel pipes, which were hammered into the fault zone (Faulkner et al., 2003; Wibberley and Shimamoto, 2003). In the laboratory, the samples were extracted by carefully cutting the steel pipes along the axis, avoiding damage to the samples as much as possible. Then the samples were dried in air, slowly and carefully to avoid the formation of shrinkage cracks, following the methods described in Hildenbrand and Urai (2003). The samples were grouped based on the macroscopic attributes and further analysed with optical microscopy, SEM, whole-rock XRD, colour measurements and high-pressure mercury porosimetry. Phase analyses by XRD were done on top-filled powder specimen. The 001 peak of the 10 Å phase (mica) was fitted with MacClayFit (Stanjek and Häusler, 2000) using a split Pseudo-Voigt function to account for asymmetry of the peak. For assessing the Kübler index (Kübler, 1990), the instrumental broadening contribution was obtained from the unweathered rock samples and was subtracted linearly from the widths of the other samples.

5. Lithotypes

We classified the material in four different lithotypes, which are interpreted to reflect different evolutionary stages of the fault zone, with associated changes in petrophysical properties in space and time. This classification, which was based on macroscopic features (Fig. 3) in the outcrop, was shown to be consistent in terms of porosity and dominant microstructures. In what follows, we describe these lithotypes in more detail.

5.1. Wall rock

The ‘wall rock’ shows no visible evidence of brittle deformation. Coherence and internal structures remain virtually unchanged. This lithotype comprises typical,

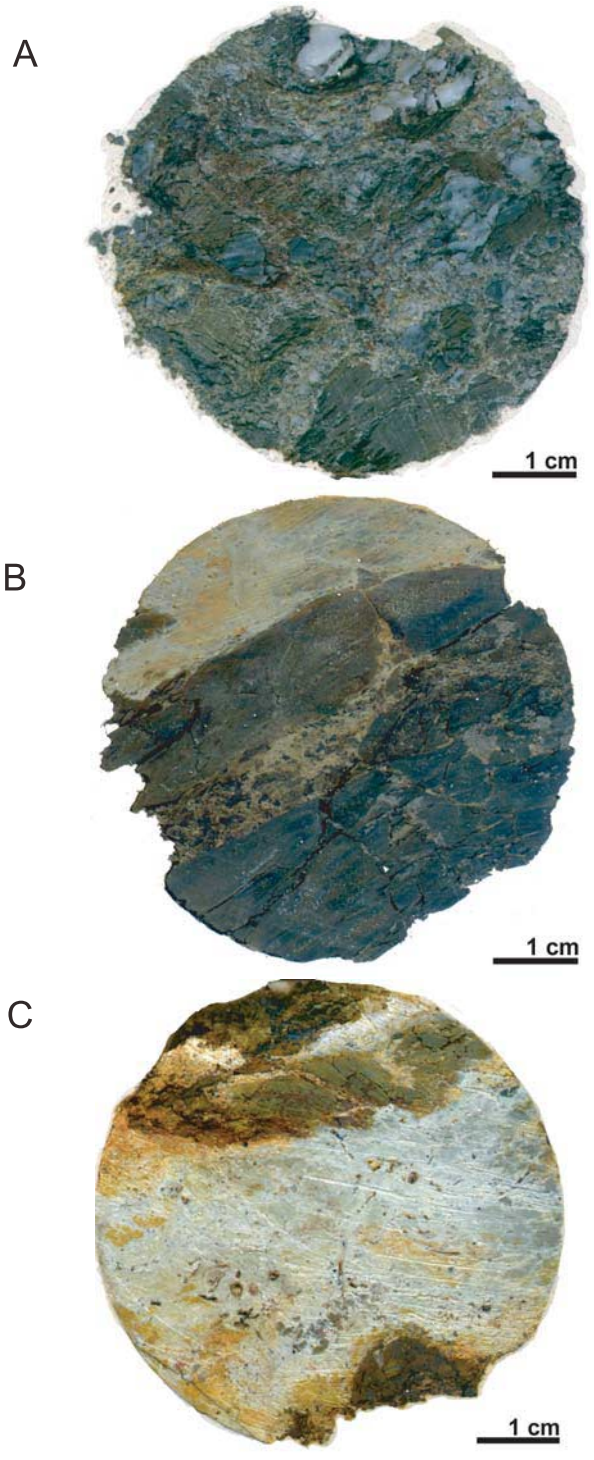

Fig. 3. Photographs of samples from different fault zone lithotypes. (A) 'Distorted rock' with a noticeable loss in coherence. Foliated fragments and Qz veins are recognizable, with abundant fracture porosity between the wall rock fragments. Sample RE2. (B) 'Transition material'. The structure of the wall rock fragments is similar to the previous, with the space between the fragments filled with clay. Sample RA3. (C) 'Clay gouge'. The dominant material is clay, with inclusions of deformed wall rock. This lithotype looks rather homogeneous in comparison with the previous types. Sample RB1.

highly overconsolidated (Ingram, 1999) fissile shale and sandstones, with low porosity and very low permeability as a result of the burial conditions.

5.2. Distorted rock

In this lithotype, the 'wall rock' is noticeably affected by brittle deformation (Fig. 3A), but original structures are clearly recognizable. Small-scale kinking, folding and fracturing are ubiquitous. The dense network of open fractures leads to a prominent loss in coherence. All fault zone lithotypes show a reddish to brown discolouring by iron oxides.

5.3. Transition material

The transition type is similar to the 'distorted rock' but with a higher content of clay-sized material (Fig. 3B). Original structures are still recognizable, but less clearly than in the 'distorted rock'. The presence of clay in between the wall rock fragments produces a noticeable increase in coherency and decrease in the amount of open fractures, in comparison with the 'distorted rock' lithotype. The distinction between 'distorted rock' and 'transition material' is subjective because it depends on the size of the area under consideration. The 'transition material' is best described as a heterogeneous mixture of the 'distorted rock' and 'clay gouge' (see below).

5.4. Clay gouge

All fault zones studied contain a significant fraction of very fine-grained 'clay gouge'. The clay is to a large extent structureless but may occasionally contain remnants of the previous material types along with broken Qz veins (Fig. 3C). The 'clay gouge' may have a sharp contact to the wall rock or it may coexist—sometimes as multiple strands—with the other lithotypes within a wider fault zone. The word 'clay' is used to indicate the mineralogical composition of the fine-grained material.

6. Mineralogy

Results of the (semi-quantitative) XRD analysis (Table 1) show a very similar composition in all samples. The mineral assemblage in Table 1 shows no distinct trends between the lithotypes, with mica and chlorite being the dominant clay minerals. Except for the wall rock samples, which showed essentially instrumental peak broadening, the widths of the 001 peak of mica varied between 0.02 and 0.11°2Θ and showed a slight (but not significant) increase of the mean (Table 2). Interpreting these widths as Kübler indices shows that none of them approaches the border value of 0.25°2Θ, which limits the epizone from shallower depths (Kübler, 1990).

Table 1
Semi-quantitative whole-rock XRD of the lithotypes sorted by the different macroscopic types

Lithotype	Taken from sample	Quartz	Kaolinite	K-feldspar	Mica	Chlorite	Goethite	Lepidokr.	Smectite
Clay gouge	S5	●●●	–	●●	●●●	–	–	–	–
	RA1	●●●	–	○	●●●	●●●	○	●●	–
	RA2	●●●	–	○	●●	●●●	○	●●	–
	RA5	●●●	–	●●	●●●	●●●	○	●●	–
	RA6	●●●	–	○	●●	●●●	○	●●	–
	RB1	●●	–	●●	●●●●	●●	○	○	○
	RB2	●●●	–	●●	●●●	○○	●●	○	○
	RB4	●●●	○	●●	●●●●	●●●	○	–	–
	RC1	●●●	–	○	●●	●●	○	○	–
Transition material	S1B2	●●●	–	●●	●●●	●●	○	–	–
	S2	●●●	–	●●	●●●	●●	○	–	–
	S4	●●●	–	●●	●●●●	●●	–	–	–
	RA4	●●●	–	●●	●●●	●●	–	●●	–
	RE3	●●●	–	●●	●●●	●●●	–	–	–
	RE4	●●●	–	●●	●●●	●●●	–	–	–
	RE6	●●●	–	○	●●	●●●	–	–	–
	RE5	●●●	–	●●	●●●	●●●	○	–	–
Distorted rock	S1B1	●●●	–	●●	●●●	●●	–	–	–
	S3	●●●	–	●●	●●●●	●●	–	–	–
	S6A	●●●	–	●●	●●●	●●	○	○	–
	RE1	●●●	–	●●	●●●●	●●●●	–	–	–
Wall rock	Srock	●●●	–	○	●●	●●	–	–	–
	RErock	●●●	–	○	●●	●●	–	–	–

●●●●, High abundance; ●●●, medium abundance; ●●, low abundance; ○, traces; –, Not detected.

Goethite and lepidocrocite showed up especially in the clay gouge samples, but goethite was detected by XRD in all groups except for the wall rock samples (Table 1). Colour measurements confirm essentially these findings with clay gouges having on average more redness (i.e. higher a^*) than the other samples (Fig. 4). This agrees with the presence of orange to brown lepidocrocite in addition to yellow goethite (Scheinost and Schwertmann, 1999). The a^* and b^* values do not indicate the presence of ferrihydrite or hematite in these samples.

7. Hg porosimetry

From the carefully dried samples, smaller (approximately 1 cm^3) samples were broken off, again avoiding damage as much as possible. These samples were used for Mercury injection, following the techniques described by Hildenbrand and Urai (2003). The Mercury injection plots (Table 1) together with Table 3 show that there are large differences between the different lithotypes. A progressive increase in the bulk porosity (Table 3) from less than 10% in the 'wall rock' to over 35% in the 'clay gouge' is a consistent trend in all samples. However, there is a large variability in the shape of the Mercury injection curves in the 'distorted rock' and 'transitional material' lithotypes, while 'wall rock' and 'clay gouge' show similar curves for all samples (Fig. 5).

Table 2
Integral widths of the 001 peak of mica (XRD) corrected for instrumental broadening

Lithotype	Count	Peak width (°2Θ), mean (SD)	*t*-Test *P* value (against wall rock)
Wall rock	2	0.00013 (3)	–
Distorted rock	4	0.0349 (1)	0.017
Transition material	8	0.0403 (6)	0.065
Clay gouge	9	0.0488 (9)	0.058

8. Microstructure in SEM

Broken surfaces of the samples were analysed with SEM to show the microstructural inventory of the lithotypes reflecting the macroscopic structure as well as the porosity distribution. The 'wall rock' is dense, and has the typical foliation of a slate (Borradaile et al., 1982). The phyllosilicates are aligned due to compaction deformation and recrystallization and show no variation at the scale of

Table 3
Median quantities derived from the Hg porosimetry

	Total porosity (vol.%)	Bulk density (g/cm^3)	No. of samples
Wall rock	9.3	2.48	2
Distorted rock	28.3	1.93	3
Transition type	27.0	2.04	9
Clay gouge	38.5	1.71	9

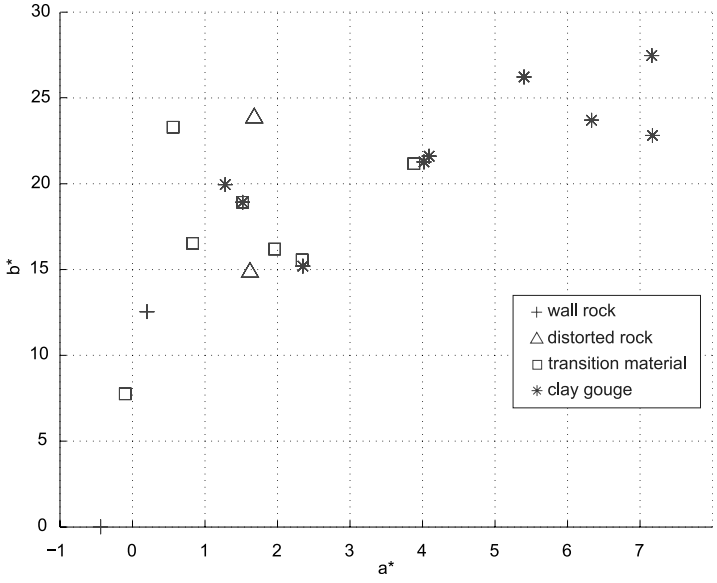

Fig. 4. Scatter plot showing the colour measurements of the red (a^*) and yellow (b^*) values of the lithotypes.

the sample (Fig. 6A). The microstructures in the 'distorted rock' contain kinked and folded foliation on a small scale, together with microcracks. This loosens the fabric and creates fracture porosity (Fig. 6B). The 'transition material' (Fig. 6C) has an increased amount of micro-fault zones and shows a decrease in the average size of the mineral components. This progressive cataclasis destroys the original fabric and fills the large pores, which are formed between the fragments in the 'deformed rock' lithotype. The 'clay gouge' consists dominantly of micrometre-sized particles (Fig. 6D) and the original fabric of the wall rock is completely obliterated. In domains, the clay particles are aligned, but there is no preferred orientation at the scale of the whole sample (10 mm). EDX measurements confirm the presence of iron oxides found in XRD.

9. Discussion

Previous work on a Devonian slate in this area (Eckhardt, 1960) describe the weathering characteristics of similar rock material. It was shown that chlorite is unstable under shallow weathering conditions and transforms into kaolinite and montmorillonite. The acidic conditions in the uppermost weathering horizon would promote the formation of kaolinite. The absence of kaolinite (except for sample RB4) and rare occurrences of smectites (RB1 and RB2) indicates, therefore, that chemical weathering processes of silicates were negligible. This is also supported by the Kübler indices, which lack significant trends across the groups. Peak widths of 0.02–0.1°2Θ would correspond to coherence lengths of 0.4–0.07 μm of the micas. Since a distinction between size broadening and strain broadening cannot be done by a single peak analysis, apparently smaller crystal sizes could also be due to strain contributions induced by physical stresses. These stresses could have induced disaggregation, but obviously did not change the primary particle size distribution to a large extent. The presence of goethite in all groups (except wall rock samples) together with lepidocrocite (mainly in the clay gouges) and the absence of ferrihydrite delimits a physicochemical environment, in which the oxidation rate of Fe^{2+} (possibly delivered by pyrite oxidation) was on the one hand slow enough to avoid ferrihydrite formation, but on the other hand fast enough to form metastable lepidocrocite (Cornell and Schwertmann, 2003). The oxidation rate of Fe^{2+} depends strongly on the solution pH and on the partial pressure of oxygen (Stumm and Morgan, 1996). For pH 6 and $PO_2 = 2.10^4$ Pa, the half-time $t_{1/2}$ for Fe^{2+} is about 7 h, whereas for pH 7 $t_{1/2}$ drops to several minutes. Although the minimum rate of Fe^{2+} oxidation for lepidocrocite formation is not known as a function of pH, we assume that for near neutral solution pH—due to silicate buffering—the oxygen supply will be rate-determining. The occurrence of lepidocrocite in many samples indicates, therefore, near surface conditions for the formation of the iron hydroxides. This implies that faulting and iron oxide formation were independent processes. The normal faults described in this project are interpreted to have offsets less than a few tens of metres, as indicated by the thickness of the fault zone, the absence of a clearly developed fault core-damage zone structure (Chester, 1993; Caine et al., 1996) and the absence of mapable offsets in the 1:25,000 geological maps of the area (Wunstorf, 1928). Therefore, the outcrops represent the small faults that are always present in a population of larger ones, and the regions near the tip of large faults. The depth of faulting is inferred to have been a few hundred metres, based on the gouge's void ratio and standard soil mechanics relationships between porosity at critical state and effective stress (Lambe and Whitman, 1969), although part of the

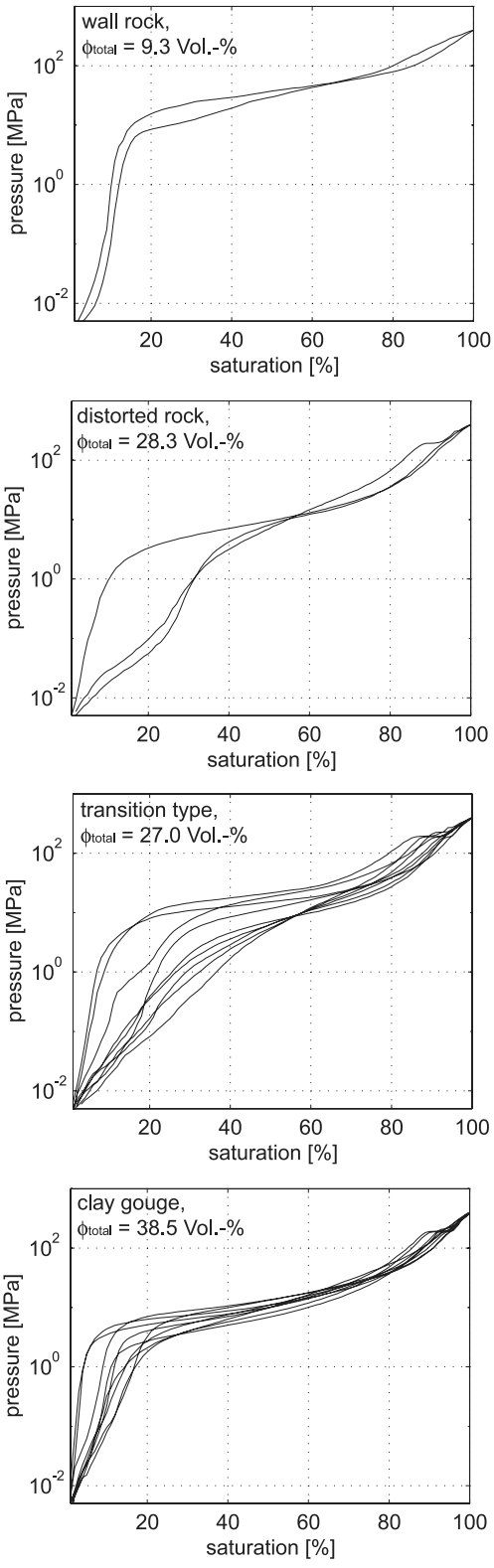

Fig. 5. Results of Hg injection experiments show the differences in the total porosity among the four types. The 'transition material' and 'distorted rock' lithotypes show a wide scatter due to the variety in different internal structures.

fault motion may well have occurred at somewhat higher depth. Considering the maximum burial depth, these rocks were extremely overconsolidated during faulting. Four different lithotypes identified in this study are interpreted to represent different evolutionary stages during progressive faulting in such systems. As expected, the spatial distribution of lithotypes is heterogeneous (Neugebauer and Simmer, 2003): a narrow band of clay gouge may laterally transfer into a wider zone with a complex distribution of all four lithotypes.

The evolution of fault gouge with progressive throw is interpreted as follows. A cohesive and strong undeformed shale (Figs. 6A and 7) with a low permeability (Fig. 5; $<$ 10 vol.% porosity; 'wall rock' type) reacts on initial faulting by a loss of cohesion due to kinking, folding and micro-fracturing of the fabric into the 'distorted rock' lithotype. The 'distorted rock' is easily recognizable (Fig. 3A) by the deformed foliation and poor coherence. The increase in porosity (to $\sim$28%; Fig. 4) is an effect of the distortion of the fabric (Fig. 6A) resulting in relatively large pores and corresponding low entry pressures (Fig. 5). This rock type may reflect the common term 'deformation zone' (Chester, 1993; Caine et al., 1996; Gudmundsson et al., 2001). Due to the dense crack network, we expect the highest permeability among the four lithotypes documented by low entry pressures in the Hg porosimetry (Figs. 5 and 7). Reddish discolouring of the deformed lithotypes might document alteration of pyrite into Fe-oxides. Progressive deformation/throw on the complex and heterogeneously spaced network of folds and cracks (Fig. 6B and C) breaks down the fabric in the stage of the 'transition material' (Fig. 3B). Abrasion lenses of the latter lithotype are mechanically scaled down, increasing the content of clay gouge material (Fig. 3B). The general decrease in grain size is associated with a denser fracture network (Fig. 6C). The total porosity hardly changes (Figs. 5 and 7), while the distribution of pore size promotes smaller diameters due to the overall reduction in grain size. The large scatter of entry pressures shown in Figs. 5 and 7 are a result of the variety in different microstructures that characterize the structural heterogeneity of the 'transition type' material. The final 'clay gouge' type (Fig. 3C) is the end member of the fault development and is dominated by an almost pure clay. Lenses of less deformed material are almost totally consumed. The clay particles are oriented in a irregular fashion (Fig. 6D) with a high porosity and small-sized pores, which is expected to reduce the overall permeability noticeably (Figs. 5 and 7). The 'clay gouge' may present the 'fault core' due to the localization of fault slip (Fig. 2). It should be noted, however, that the clay gouge occasionally forms complex networks of anatomising bands, sometimes branching off the main fault plane (Fig. 2) rather than a localized, subplanar slip-plane. The whole-rock XRD analysis shows similar compositions among the four lithotypes. A noticeable increase in Fe-bearing minerals is evident due to the alteration of pyrite—macroscopically shown by brownish to

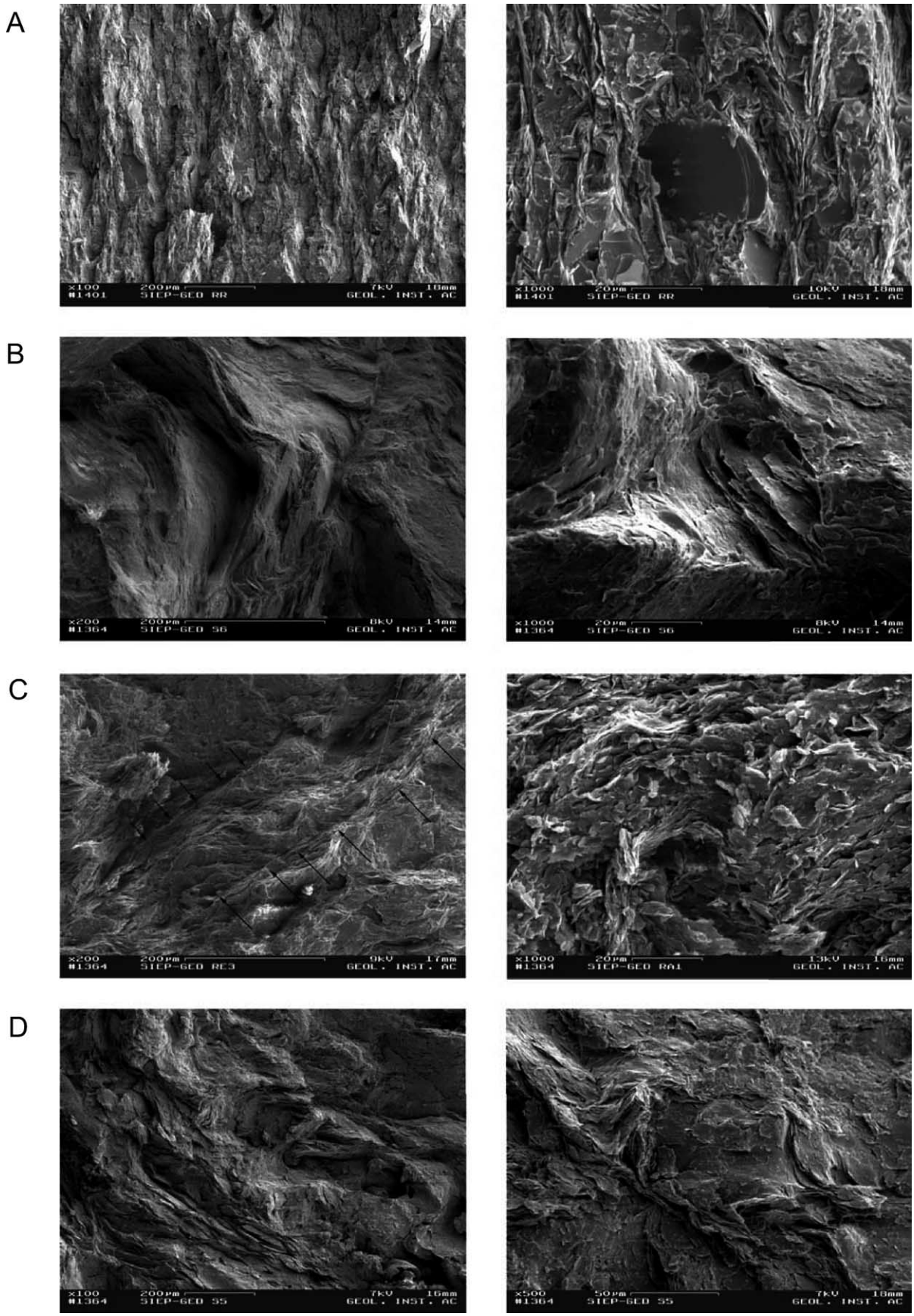
A
B
C
D

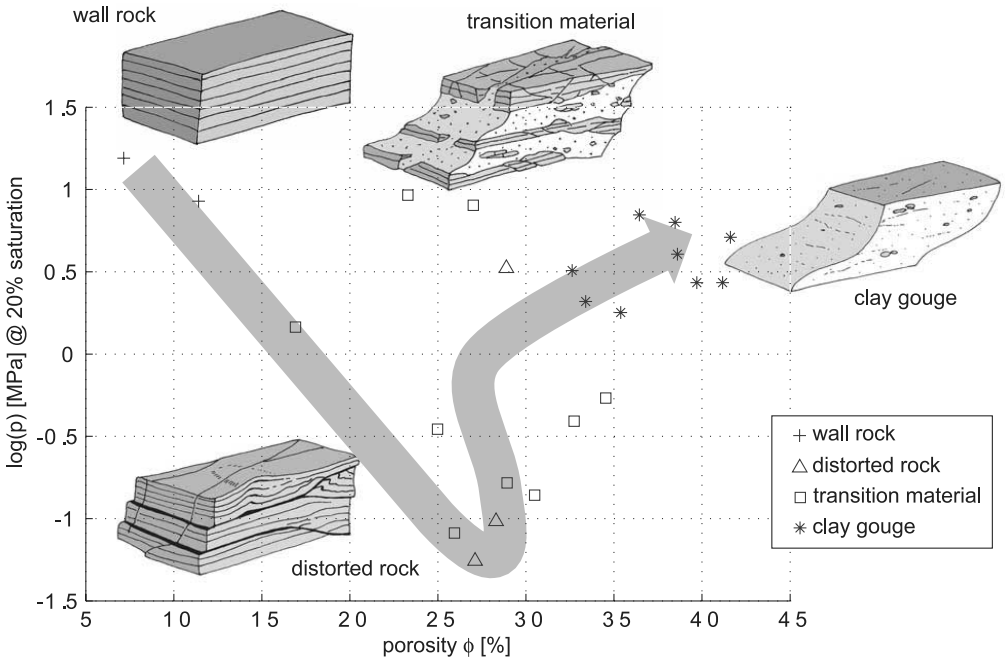

Fig. 7. Evolutionary model of the development of the lithotypes. The axes show the logarithm of the Hg injection pressure (at 20% saturation) versus the bulk porosity (vol.%). The 'wall rock' responds to the faulting process by a general loss in coherence. Microcracks and kinks ('distorted rock') create large pores (low entry pressures). Progressive deformation leads to an increase in entry-pressures interpreted as a mechanical breakdown of the mineral fragments ('transition material'). The large scatter of the 'transition material' is due to the variety of possible microstructures. The final stage is the 'clay gouge'. The mechanical breakdown at shallow depth ends with a large volume of small pores. Despite the high porosity, the initial entry pressure is almost recovered.

reddish discolouring. The chlorite content of the wall rock sustains in the deformation process, while smectite and kaolonite are negligible. This excludes (Eckhardt, 1960) surface-related weathering processes and suggests that the deformation stages documented are of pure mechanical nature.

10. Conclusions

The mechanical destruction of the overconsolidated claystone involves the initial failure of the fabric ('distorted rock'; Fig. 7) with permeable pathways, its break-up into clay fractions ('transition rock'; Fig. 7) and the progressive milling into a pure 'clay gouge' (Fig. 7) with an approximate restoration of the entry pressures. The microstructural evolution (Fig. 7), as well as the heterogeneous special distribution (Fig. 2) of the lithotypes, suggests a complex permeability development within this lithology on the basis of mechanical processes. The main process involved in the evolution of these faults is mechanical fragmentation with only minor contribution by diagenetic changes or weathering. The large changes in the microstructures affect the mechanical strength, porosity and transport properties. This results in an early increase in porosity and a later decrease within distinct zones. Since the proposed lithotypes may coexist, brittle faulting of overconsolidated materials may lead to an early re-sealing within claystone sections, creating local barriers to along-fault fluid flow. The associated anisotropies in relative strength and transport properties may play an important role in the characterisation of low-offset faults during the exhumation of siliclastic sedimentary basins.

Acknowledgements

We thank B. Fitzner and colleagues of the Working group 'Natural stones and weathering' at RWTH Aachen for the Hg porosimetry measurements and the support on the SEM work as well as F.M. Meyer and colleagues of the 'Institute of Mineralogy and Economic Geology' at RWTH Aachen for the XRD work. Shell research is thanked for sponsorship on this project. C. Wibberley and an anonymous reviewer are thanked for their constructive reviews.

Fig. 6. SEM images from the four lithotypes at different magnifications. (A) 'Wall rock' with undisturbed parallel foliation. (B) 'Distorted rock' with kinks and folds. (C) Small fracture zones (arrows) in the 'transition material' promote the mechanical grain size reduction. (D) Chaotic fabric in the 'clay gouge' type with small mineral components and a high porosity. (Scale bars are: on the left 200 μm and on the right 20 and 50 μm.)

References

Billi, A., Salvini, F., Storti, F., 2002. The damage zone–fault core transition in carbonate rocks: implications for fault growth, structure and permeability. Journal of Structural Geology 25 (11), 1779–1794.

Borradaile, G.J., Bayly, M.B., Powell, C.M., 1982. Atlas of Deformational and Metamorphic Rock Fabrics. Springer, Berlin.

Caine, J.S., Evans, J.P., Forster, C.B., 1996. Fault zone architecture and permeability structure. Geology 24 (11), 1025–1028.

Chester, F.M., 1993. Internal structure and weakening mechanisms of the San Andreas Fault. In: Evans, J.P., Biegel, R.L. (Eds.), Journal of Geophysical Research, vol. 98. American Geophysical Union, Washington, DC, p. 771.

Cornell, R.M., Schwertmann, U., 2003. The Iron Oxides. Wiley, New York.

Eckhardt, F.J., 1960. Die Veraenderungen eines devonischen Tonschiefers durch die Mineralumwandlungen infolge der tertiaeren Zersetzung. Zeitschrift der Deutschen Geologischen Gesellschaft 112 (1), 188.

Evans, J.P., Forster, C.B., Goddard, J.V., 1997. Permeability of fault-related rocks, and implications for hydraulic structure of fault zones. Journal of Structural Geology 19 (11), 1393–1404.

Faulkner, D.R., Lewis, A.C., Rutter, E.H., 2003. On the internal structure and mechanics of large strike-slip fault zones: field observations of the Carboneras fault in southeastern Spain. Tectonophysics 367 (3/4), 235–251.

Fuchs, K., von Gehlen, K., Maelzer, H., Murawski, H., Semmel, A. (Eds.), 1983. Plateau Uplift—The Rhenish Shield—A Case History. Springer, Berlin, p. 411.

Gudmundsson, A., Berg, S.S., Lyslo, K.B., Skurtveit, E., 2001. Fracture networks and fluid transport in active fault zones. Journal of Structural Geology 23 (2/3), 343–353.

Hildenbrand, A., Urai, J.L., 2003. Investigation of the morphology of pore space in mudstones—first results. Marine and Petroleum Geology 20 (10), 1185–1200.

Ingram, G.M., 1999. Top-seal leakage through faults and fractures; the role of mudrock properties. In: Urai, J.L. (Ed.), Geological Society Special Publications, vol. 158. Geological Society of London, United Kingdom, p. 125.

Jones, M., 1994. Mechanical principles of sediment deformation. In: Maltman, A. (Ed.), The Geological Deformation of Sediments. Chapman & Hall, London, pp. 37–71.

Jones, M.E., Addis, M.A., 1986. The application of stress path and critical state analysis to sediment deformation. Journal of Structural Geology 8 (5), 575–580.

Knipe, R.J., 1992. Faulting processes and fault seal. Norwegian Petroleum Society NPF Special Publication, vol. 1. Elsevier, New York, p. 325.

Kralik, M., Klima, K., Riedmueller, G., 1987. Dating fault gouges. Nature 326 (6120), 315–317.

Kramm, U., 1982. Die Metamorphose des Venn-Stavelot-Massivs, nordwestliches Rheinisches Schiefergebirge: Grad Alter und Ursache. Dechiniana 135, 121–178.

Kübler, B., 1990. 'Cristallinité' de l'illite et mixed-layers: breve révision. Schweizerische Mineralogische und Petrographische Mitteilungen 70, 89–93.

Lambe, T.W., Whitman, R.V., 1969. Soil Mechanics. Wiley, New York.

Lindsay, N.G., 1993. Outcrop studies of shale smears on fault surfaces. In: Murphy, F.C., Walsh, J.J., Watterson, J. (Eds.), Special Publication of the International Association of Sedimentologists, vol. 15. Blackwell, Oxford, p. 113.

Mollema, P.N., Antonellini, M., 1999. Development of strike-slip faults in the dolomites of the Sella Group, Northern Italy. Journal of Structural Geology 21 (3), 273–292.

Neugebauer, H.J., Simmer, C. (Eds.), 2003. Dynamics of Multiscale Earth Systems. Springer, Berlin.

Nüesch, R., 1991. Das mechanische Verhalten von Opalinuston. Unpublished PhD Thesis, ETH Zürich.

Nüesch, R., Baumann, W., 1989. Ton- und Sulfatgesteine in Wechselwirkung bei Deformation. Geologische Rundschau 78 (2), 443–457.

Olgaard, D.L., Nüesch, R., Urai, J., 1995. Consolidation of water saturated shales at great depth under drained conditions. In: Fujii, T. (Ed.), Eighth International Congress on Rock Mechanics, Tokyo, Japan, p. 5.

Rawling, G.C., 2001a. Internal architecture, permeability structure, and hydrologic significance of contrasting fault-zone types. In: Goodwin, L.B., Wilson, J.L. (Eds.), Geology Boulder, vol. 29. Geological Society of America (GSA), Boulder, CO, p. 43.

Rawling, G.C., 2001b. The nature of cataclastic deformation and its structural and hydrologic implications, Sand Hill fault zone, Albuquerque Basin, New Mexico, USA. In: Goodwin, L.B. (Ed.), Abstracts with Programs—Geological Society of America, vol. 33. Geological Society of America (GSA), Boulder, CO, p. 8.

Scheinost, A., Schwertmann, U., 1999. Color identification of iron oxides and hydrosulfates: use and limitations. Soil Science Society of America Journal 63, 1462–1471.

Shipton, Z.K., Cowie, P.A., 2001. Damage zone and slip-surface evolution over μm to km scales in high-porosity Navajo sandstone, Utah. Journal of Structural Geology 23 (12), 1825–1844.

Stanjek, H., Häusler, W., 2000. Quantifizierung silikatischer Tonminerale im Textur und Pulverpräperaten mit MacClayFit. Berichte der Deutschen Ton- und Tonmineralgruppe 7, 256–265.

Stumm, W., Morgan, J.J., 1996. Aquatic Chemistry. Wiley, New York.

Urai, J.L., Wong, S.W., 1994. Deformation mechanisms in experimentally deformed shales. European Geophysical Union Annual Meeting, Grenoble, Annales Geophysicae, 12.

Vajdova, V., Baud, P., Wong, T.-F., 2004. Compaction, dilatancy, and failure in porous carbonate rocks. Journal of Geophysical Research 109 (B05204).

Walter, R., 1992. Geologie von Mitteleuropa. E.Schweizerbart'sche Verlagsbuchhandlung, Stuttgart.

Walter, R., Wohlenberg, J., 1985. Geology and Geophysics of the Northeastern Hohes Venn Area. E.Schweizerbart'sche Verlagsbuchhandlung, Stuttgart.

Wibberley, C.A.J., Shimamoto, T., 2003. Internal structure and permeability of major strike-slip fault zones: the Median Tectonic Line in Mie Prefecture, Southwest Japan. Journal of Structural Geology 25 (1), 59–78.

Wunstorf, W., 1928. Geologische Karte des deutschen Reiches 1:25000, Blatt Nideggen. Preußisches Geologisches Landesamt, Berlin.